Inorganic Chemistry

Article

pubs.acs.org/IC

Synthesis of Chelating Complexes through Solid-State Dehydrochlorination Reactions via Second-Sphere-Coordination Interaction with Metal Chlorides: A Combined Experimental–Molecular Modeling Study

Hong-yu Guan,[†] Zhen Wang,[†] Antonino Famulari,[‡] Xu Wang,[†] Fang Guo,*[,†] and Javier Martí-Rujas*[,§]

[†]College of Chemistry, Liaoning University, Shenyang 110036, China

[‡]Dipartimento di Chimica Materiali e Ingegneria Chimica "Giulio Natta", Politecnico di Milano, Via L. Mancinelli 7, 20131 Milan, Italy

[§]Center for Nano Science and Technology, Istituto Italiano di Tecnologia (ITT@Polimi), Via Pascoli 70/3, 20133 Milano, Italy

Supporting Information

ABSTRACT: We have applied crystal engineering as a tool to study the solid-state transformation from molecular salts to coordination complexes via mechanochemical dehydrochlorination reactions. The $-(CH_2)_n-$ (n = 2, 3) alkyl chains were introduced into the bibenzylamine moiety to form the two nitrogen bases *N*,*N*,*N*′,*N*′-tetrabenzylethylenediamine ($\mathbf{L^1}$) and *N*,*N*,*N*′,*N*′-tetrabenzylpropydiamine ($\mathbf{L^2}$), which were self-assembled with tetrachlorometalates to form a series of supramolecular salts through second-sphere coordination. Single crystals of salts $[\mathbf{L^1}]2H^+\cdot[CuCl_4]^{2-}\cdot$solvent (**1**) and $[\mathbf{L^2}]2H^+\cdot[XCl_4]^{2-}\cdot$solvent (**2**–**4**; X = Cu, Hg, Zn) were obtained and their structures determined by single-crystal X-ray diffraction. The effect of different alkyl chains (two and three $-CH_2-$ units) on the solid-state reactivity showed that the chelating complexes resulting from the mechanochemical dehydrohalogenation reaction depend on the formation of *quasi*-chelating hydrogen-bonding salts. Quantum-mechanical calculations have been used to gain insight in this mechanochemical dehydrohalogenation reaction, demonstrating that not only is size matching between reactants is important but also conformational energies, intermolecular interactions, and the symmetry of frontier molecular orbitals play an important role.

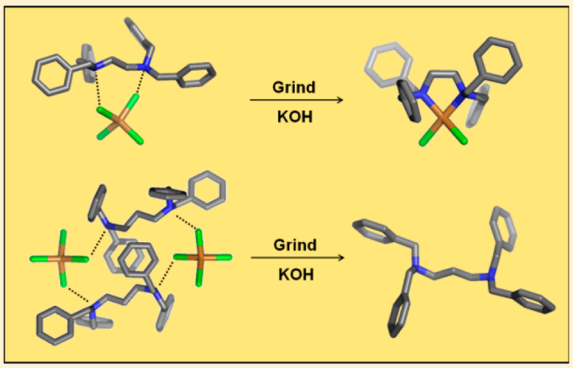

INTRODUCTION

Controlling supramolecular self-assembly through crystal engineering is one of the most important issues in modern solid-state chemistry. Weak interactions are crucial in the molecular self-assembling outcome, and its control is hard to predict.[1] Crystals are, in fact, the result of a fine balance of intramolecular and intermolecular subtle effects. Crystal engineering of various molecular components, either organic or mixed metal–organic assembled only by weak intermolecular forces, has led to significant advances in areas like improved pharmaceutical properties,[2] gas adsorption,[3] semiconductors,[4] and molecular transport.[5] A crucial aspect in many solid-state reactions is the orientation and distance between reactants, which often means that the crystalline environment can induce a high degree of regio- and stereoselectivity control. The separation distance, mutual orientation, and space symmetry of reactive functional groups are crucial in solid-state chemistry.

The use of organic cations and metal ions via second-sphere coordination to construct host frameworks with accessible voids/spaces for inclusion of guest molecules was already mentioned by Stoddart et al. in the early 1980s[6] and, more recently, has been exploited by Loeb et al.[7] The construction of second-sphere coordination refers to any intermolecular interactions with the ligands directly bound to the primary coordination sphere of a metal ion. On the basis of this strategy, some urea(amido)-containing ligands have been applied as extractants for highly selective extraction of $[PtCl_6]^{2-}$, $[ZnCl_4]^{2-}$, and $[CoCl_4]^{2-}$ and, more recently, using α-cyclodextrin for gold recovery.[8,9] Halogen bonds[10] have also been used recently to construct second-sphere coordination isostructural (6,3)-networks able to form adducts with a mixture of mononegative tetrahedral oxyanions.[11]

We recently reported the solid-state mechanochemical dehydrohalogenation reaction starting from salts assembled by second-sphere coordination.[12] However, the solid-state chemistry of second-sphere-coordination networks is still a

Received: April 2, 2014
Published: June 24, 2014

   dx.doi.org/10.1021/ic5007583 | *Inorg. Chem.* 2014, 53, 7438–7445

research field that remains relatively unexplored, particularly if compared with that of metal−organic frameworks.[13] Reports studying fundamental solid-state reactions involving second-sphere-coordination complexes are important because they can help in the development of such hybrid metal organic adducts toward new functional crystalline materials.[14]

Herein, we report a series of supramolecular structures obtained using second-sphere coordination and their solid-state chelation upon mechanochemical dehydrochlorination.[15] We have synthesized two bidentate ligands ($\mathbf{L^1}$ and $\mathbf{L^2}$) by introducing $-(CH_2)_n-$ alkyl chains on the bibenzylamine ligand at the N atom through covalent bonds (Scheme 1a). We

Scheme 1. Cartoon Showing the Ligands $\mathbf{L^1}$ and $\mathbf{L^2}$ (a) and Their Mechanochemical Dehydrochlorination Reactions with $[CuCl_4]^{2-}$ (b and c)

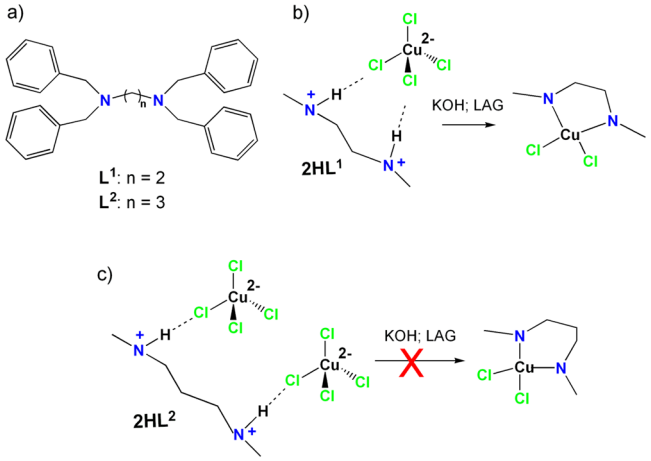

demonstrate that the chelating reaction upon dehydrochlorination depends on the length of the chelating backbone in ligands $\mathbf{L^1}$ and $\mathbf{L^2}$ (Scheme 1b,c). Moreover, using structural models obtained from single-crystal X-ray diffraction (XRD), quantum-mechanical (QM) calculations also including methods specific for solid phases were carried out to gain insight into molecular conformations, intermolecular interactions, and the electronic density distribution of frontier molecular orbitals (FMOs) in ligands $\mathbf{L^1}$ and $\mathbf{L^2}$. To our best knowledge, the successful application of crystal engineering to the formation of chelating complexes by mechanochemical solid-state reactions through second-sphere coordination has not been reported, and the effect of $-(CH_2)_n-$ spacers on the formation of various second-sphere complexes has not been investigated using such large and flexible organic cations. Additionally, we combined experimental and molecular modeling to gain insight into these uncommon mechanochemical transformations. The approach used herein can pave the way to understanding mechanochemical reactions and the possible mechanisms behind it in this area of coordination chemistry.

EXPERIMENTAL SECTION

Materials and Methods. All chemicals were obtained from commercial sources and used without further purification. IR spectra were obtained with a PerkinElmer 100 FT-IR spectrometer using KBr pellets. ^{1}H NMR spectra were recorded on a Mercury-Plus 300 spectrometer (Varian, 300 MHz) at 25 °C with tetramethylsilane as the internal reference.

Single-crystal data collection of **1**, **3**, and **4** was performed on a Bruker P4 diffractometer with Mo Kα radiation (λ = 0.71073 Å). The diffraction data for $\mathbf{L^2}$, **1′**, and **2** were recorded with a Bruker X8 Prospector APEX-II/CCD diffractometer equipped with a focusing mirror (Cu Kα radiation; λ = 1.54056 Å). The structures were determined using direct methods and refined (based on F^2 using all independent data) by full-matrix least-squares methods (*SHELXTL 97*).[16] All non-H atoms were located from difference Fourier maps and refined with anisotropic displacement parameters. Powder XRD (PXRD) was recorded on a D2 Bruker diffractometer (λ = 1.54056 Å) in reflection mode.

Preparation of Ligands $\mathbf{L^1}$ and $\mathbf{L^2}$. *Preparation of $\mathbf{L^1}$.* A total of 7 mL of ethylenediamine was slowly added to a solution of 8 g of NaOH and 20 mL of distilled water. A total of 30 mL of benzyl chloride (2−3 drops) was then continuously added to the mixture solution. Then, the reaction was heated to 95 °C and stirred for 4 h. The mixture was cooled to room temperature. The white reaction product was separated from diethyl ether and then washed with distilled water. Recrystallization using anhydrous ethanol (EtOH) and drying in vacuo produced white crystals. Yield: 12.43 g, 60.0%. Mp: 98−100 °C. ^{1}H NMR ($CDCl_3$, 300 MHz): δ 2.60 (2H, s, CH_2), 3.50 (4H, s, CH_2), 7.23−7.27 (10H, m, ArH).

Preparation of $\mathbf{L^2}$. A total of 4.2 mL of 1,3-propanediamine was slowly added to a solution of 8 g of NaOH and 18 mL of anhydrous EtOH. A total of 27.5 mL of benzyl chloride (2−3 drops) was then continuously added to the mixture solution. Then, the reaction was heated to 80 °C and stirred for 4 h. The mixture was cooled to room temperature. The white reaction product was separated from EtOH and then washed with distilled water several times. White needle crystals were obtained upon recrystallization using anhydrous EtOH upon mild heating and drying in vacuo. Yield: 14.06 g, 64.6%. Mp: 50.6−51.3 °C. ^{1}H NMR ($CDCl_3$, 300 MHz): δ 1.71 (2H, s, CH_2), 2.38−2.42 (4H, t, CH_2), 3.48 (8H, s, CH_2), 7.21−7.28 (20H, m, ArH).

Preparation of Crystal 1. A total of 350 mg (0.8 mmol) of $\mathbf{L^1}$ and 10 mL of EtOH were placed in a 50 mL Erlenmeyer flask, then 190 mg of $CuCl_2{\cdot}2H_2O$ (11 mmol) and 1 mL of concentrated hydrochloric acid were slowly added, and the flask was shaken until the contents were dissolved. The flask was allowed to stand for about 8−10 days at room temperature, giving rise to orange crystals of **1** suitable for crystallographic studies.

Preparation of Crystals 2−4. A total of 100 mg (0.2 mmol) of $\mathbf{L^2}$ and 20 mL of EtOH were placed in a 50 mL Erlenmeyer flask, then 190 mg of $CuCl_2{\cdot}2H_2O$ (1.1 mmol) and 1 mL of concentrated hydrochloric acid were slowly added, and the flask was shaken until the contents were dissolved. The flask was allowed to stand for nearly 1 month at room temperature, giving rise to red block crystals (**2**) suitable for crystallographic studies.

A total of 10 mg of $\mathbf{L^2}$ (0. 02 mmol) and 8 mL of methanol (MeOH) were placed in a 25 mL Erlenmeyer flask, then 10 g of $HgCl_2$ (0.04 mmol) and 0.05 mL of concentrated hydrochloric acid were slowly added, and the flask was shaken until the contents were dissolved. The flask was allowed to stand for over 1 week at room temperature, giving rise to colorless crystals (**3**) suitable for crystallographic studies.

A total of 10 mg of $\mathbf{L^2}$ (0. 02 mmol) and 8 mL of MeOH were placed in a 25 mL Erlenmeyer flask, then 10 mg of $ZnCl_2$ (0. 07 mmol) and 0.05 mL of concentrated hydrochloric acid were slowly added, and the flask was shaken until the contents were dissolved. The flask was allowed to stand for 2−3 days at room temperature, giving rise to colorless crystals (**4**) suitable for crystallographic studies.

Solid-State Reaction. Liquid-assisted grinding (LAG) of 21 mg (0.033 mmol) of **1** and 3.7 mg (0.066 mmol) of KOH in a 1:2 molar ratio, with the addition of 30 μL of MeOH, was carried out. Upon grinding, a color change from orange to dark green was observed within 5 min.

Synthesis of Crystal 1′. The ligand $\mathbf{L^1}$ was disolved in 5 mL of EtOH, which was slowly added to a solution of $CuCl_2{\cdot}2H_2O$ (42.5 g, 0.25 mmol) in 5 mL of EtOH. The system became turbid and a precipitate was observed. The solution continued to stir for 30 min, and then stood overnight at room temperature. After filtration, the

dx.doi.org/10.1021/ic5007583 | Inorg. Chem. 2014, 53, 7438−7445

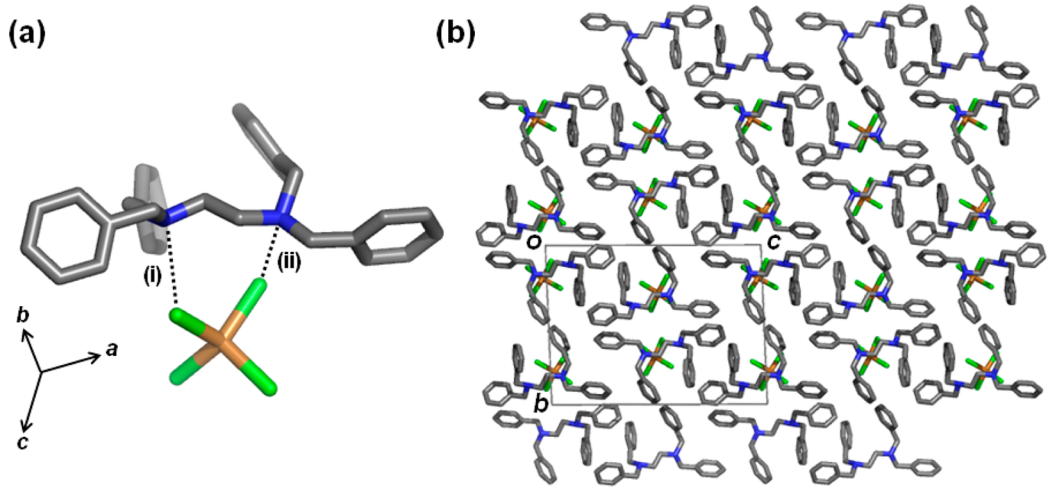

Figure 1. Crystal **1** formed by $\mathbf{L}^1$ and $[CuCl_4]^{2-}$. (a) *Quasi*-chelating hydrogen-bonding interaction between the dianion and dication. (b) Packing of salt **1** viewed along the *a* axis. Guest molecules and H atoms are omitted for clarity.

residue was washed with EtOH and dried at 50−55 °C to give large dark-green crystals of **1′**. Yield: 128.5 mg, 87%. Mp: 106−108 °C.

Crystallography. *Single-crystal data for* $\mathbf{L}^2$*:* monoclinic, space group $P2_1/c$, a = 19.043(2) Å, b = 5.7815(7) Å, c = 23.610(2) Å, β = 109.678(6)°, V = 2447.6(5) Å^3, D_c = 1.179 g cm^{-3}, R_{int} = 0.0451, $F(000)$ = 936, 13410 total reflections, 4130 unique reflections, and 2887 observed reflections with $I > 2.0\ \sigma(I)$, R1 = 0.0458, wR2 = 0.188, R2 (all data) = 0.1213, S = 1.121, T = 150 K, CCDC 994116.

Single-crystal data for ***1****:* triclinic, space group $P\bar{1}$, a = 9.318(4) Å, b = 15.815(7) Å, c = 21.419(10) Å, α = 92.167(9)°, β = 92.094(9)°, γ = 90.933(9)°, V = 3151(2) Å^3, D_c = 1.353 g cm^{-3}, R_{int} = 0.0705, $F(000)$ = 1328, 16022 total reflections, 10844 unique reflections, and 3978 observed reflections with $I > 2.0\ \sigma(I)$, R1 = 0. 0785, wR2 = 0.2130, R2 (all data) = 0.2296, S = 0.943, T = 293 K, CCDC 994117.

Single-crystal data for ***1′****:* orthorhombic, space group *Pbcn*, a = 9.9271(13) Å, b = 13.0258(17) Å, c = 21.325(3) Å, V = 2757.5(7) Å^3, D_c = 1.337 g cm^{-3}, R_{int} = 0.127, $F(000)$ = 1156, 8537 total reflections, 2322 unique reflections, and 1112 observed reflections with $I > 2.0\ \sigma(I)$, R1 = 0.073, wR2 = 0.2223, R2 (all data) = 0.1236, S = 0.863, T = 298 K, CCDC 994118.

Single-crystal data for ***2****:* monoclinic, space group $P2_1/n$, a = 13.4266(17) Å, b = 18.462(2) Å, c = 13.5988(18) Å, β = 91.929(6)°, V = 3368.99(8) Å^3, D_c = 1.345 g cm^{-3}, R_{int} = 0.0346, $F(000)$ = 1412, 18599 total reflections, 5700 unique reflections, and 5031 observed reflections with $I > 2.0\ \sigma(I)$, R1 = 0.0453, wR2 = 0.1325, R2 (all data) = 0.0505, S = 1.064, T = 150 K, CCDC 994119.

Single-crystal data for ***3****:* monoclinic, space group $P2_1/c$, a = 9.0210(18) Å, b = 11.826(2) Å, c = 30.945(6) Å, β = 91.46(3)°, V = 3300.1(11) Å^3, D_c = 1.600 g cm^{-3}, R_{int} =0.1071, $F(000)$ = 1572, 22889 total reflections, 7553 unique reflections, and 5456 observed reflections with $I > 2.0\ \sigma(I)$, R1 = 0.0685, wR2 =0.1835, R2 (all data) = 0.0938, S = 1.021, T = 113 K, CCDC 994114.

Single-crystal data for ***4****:* monoclinic, $C2/c$, a = 10.976(18) Å, b = 16.39(3) Å, c = 19.97(4) Å, β = 97.652(17)°, V = 3560(11) Å^3, D_c = 1.317 g cm^{-3}, R_{int} = 0.0296, $F(000)$ = 1448, 7041 total reflections, 3048 unique reflections, and 2330 observed reflections with $I > 2.0\ \sigma(I)$, R1 = 0.0630, wR2 = 0.2023, R2 (all data) = 0.0791, S = 1.111, T = 296 K, CCDC 994115.

RESULTS AND DISCUSSION

***Quasi*-Chelating Hydrogen-Bonding Motif in 1 and Its Transformation to the Coordination Complex 1′ in the Solid State.** In order to study a new mechanochemical dehydrochlorination reaction using a large and flexible molecule, the ligand $\mathbf{L}^1$ with a N−$(CH_2)_2$−N backbone between the two bulky dibenzylamine moiety chains was synthesized[17] and self-assembled with $[CuCl_4]^{2-}$ using second-sphere coordination. We note that the N−N distance in the crystalline structure of $\mathbf{L}^1$ is 3.766 Å.[18] The diffusion of a solution of $CuCl_2{\cdot}2H_2O$ in EtOH into a HCl/EtOH solution of $\mathbf{L}^1$ resulted in the salt $[\mathbf{L}^1]2H^+{\cdot}[CuCl_4]^{2-}{\cdot}$EtOH (**1**). In **1**, there are two $[CuCl_4]^{2-}$ dianions, two doubly protonated $\mathbf{L}^1$, and one EtOH molecule in each asymmetric unit.[19] Clearly, a specific ionic recognition between the doubly protonated $\mathbf{L}^1$ and the $[CuCl_4]^{2-}$ anion occurs. The two N protons in one independent $\mathbf{L}^1$ are linked with the same $[CuCl_4]^{2-}$ anion through two charge-assisted N−H···Cl hydrogen bonds i and ii [i, N1−H1···Cl2 with distance $d_{N1\cdots Cl2}$ = 3.166(7) Å and angle N1−H41···Cl2 = 156.8(2)°; ii, N2−H2···Cl1 with distance $d_{N2\cdots Cl1}$ = 3.151(6) Å and angle N2−H2···Cl1 = 172.0(4)°] in one cation−anion couple. For the second cation−anion couple, the other independent $\mathbf{L}^1$ forms the charge-assisted hydrogen bonds iii and iv [iii, N3−H3···Cl7 with distance $d_{N3\cdots Cl7}$ = 3.166(7) Å and angle N3−H3··Cl7 = 157.7(4)°; iv, N4−H101···Cl5 with distance $d_{N4\cdots Cl5}$ = 3.130(7) Å and angle N4−H101···Cl5 = 171.4(4)°]. The above interactions form a *quasi*-chelating[20] interaction motif (Figure 1a).[21] The *quasi*-chelating units are connected to adjacent dications through three C−H···Cl interactions, forming a hydrogen-bonded chain along the *a* axis (Figures S2 and S3 in the Supporting Information, SI). The two neighboring hydrogen-bonded chains accommodate EtOH molecules. The guest molecules do not form continuous channels but confined voids.

Dehydrochlorination reactions consisting of the removal of HCl from crystalline salts have been rarely investigated in coordination molecular complexes.[22,23] The *quasi*-chelating salt **1** can provide an opportunity to study the transformation from a hydrogen-bond salt network to a coordination complex via dehydrochlorination. That is, it is possible to study whether the orientation of the reactants (i.e., cations and anions) is favorable to form a chelated system.

In the doubly protonated $\mathbf{L}^1$, the two methylene groups $[(CH_2)_n$ $(n = 2)]$ inserted between two dibenzylamine moieties result in the two N donors separated approximately by 3.683 Å, and such a distance (i.e., about 0.1 Å), shorter than the corresponding distance in a neutral ligand, seems appropriate for chelation to occur. LAG[24] of powders of **1** and KOH in a 1:2 molar ratio rapidly showed a color change (i.e., from yellow to green) within 5 min (Figure 2). PXRD of the powder

dx.doi.org/10.1021/ic5007583 | Inorg. Chem. 2014, 53, 7438−7445

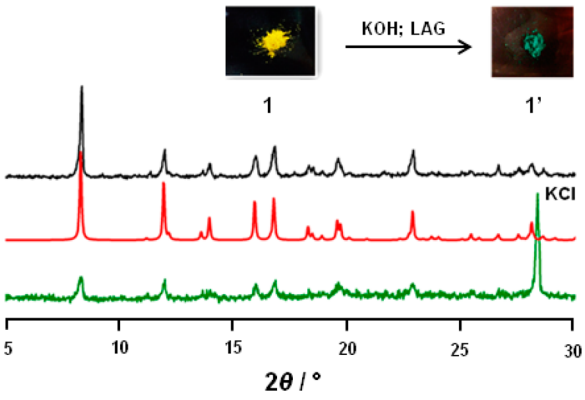

Figure 2. Pictures of the actual microcrystals of **1** and **1′** after dehydrochlorination. Comparison of the PXRD patterns: solution synthesis of **1′** from EtOH (black), simulated from single crystals (red), and the crude product including the product phase, KCl (green).

product indicated that a new phase and byproduct KCl (2θ = 28°) had been formed (Figure 2). Recrystallization of the product obtained by grinding yields suitable crystals for single-crystal XRD analysis. The match between the PXRD pattern obtained by grinding and that simulated from single-crystal XRD data suggests that the bulk powder has the same structure as the one obtained from the single crystal.

X-ray structure determination from single crystals confirms that salt **1** transformed to the neutral metal coordination complex $(CuCl_2)(L^1)$ (**1′**) upon dehydrochlorination. In the transformation from **1** to **1′**, disruption of weaker noncovalent charge-assisted N−H···Cl hydrogen bonds took place, while new Cu−N coordination bonds were formed upon chelation (Figure 3). The space group changed from triclinic ($P\bar{1}$) to orthorhombic (*Pbcn*) after dehydrochlorination. The main changes in the lattice parameters correspond to the shortening of the *b* axis (from 15.815 to 13.026 Å) and the change in the α and β angles (from 92.167° to 90° for α and from 92.094° to 90° for β). The hydrogen-bonded chain along the *a* axis in crystal **1** was transferred to coordination complex **1′** through C−H···Cl interactions (Figure 3). No inclusion of guest molecules in **1′** was observed. It is known that in some cases dehydrochlorination can occur upon heating.[22b] We tested whether dehydrochlorination followed by chelation in **1** takes place upon heating. As observed by PXRD (see Figure S6 in the SI), complex **1′** was not formed even upon heating to 200 °C.

Structural Diversity of Hydrogen-Bonding Motifs in L^2 Salts and Their Mechanochemical Reactivity in the Solid State. In order to gain insight into how the distances and orientation of the reacting partners (i.e., cations and anions) affect the mechanochemical dehydrochlorination reaction, we synthesized a new ligand (L^2) with a longer $-N-(CH_2)_3-N-$ backbone by inserting an extra methylene spacer into L^1.[25] Single-crystal X-ray structure determination of L^2 showed that the N−N distance in the propylenediamine backbone is ca. 5.113 Å. Under the same crystallization conditions as those used to crystallize **1**, a new salt (**2**) was obtained by mixing flexible L^2 and $CuCl_2{\cdot}2H_2O$ in EtOH.

Salt **2** crystallizes in the monoclinic $P2_1/n$ space group comprising one molecule of doubly protonated ligand L^2, one $[CuCl_4]^{2-}$ anion, and one molecule of EtOH in the asymmetric unit. As shown in Figure 4, one $[CuCl_4]^{2-}$ is hydrogen-bonded

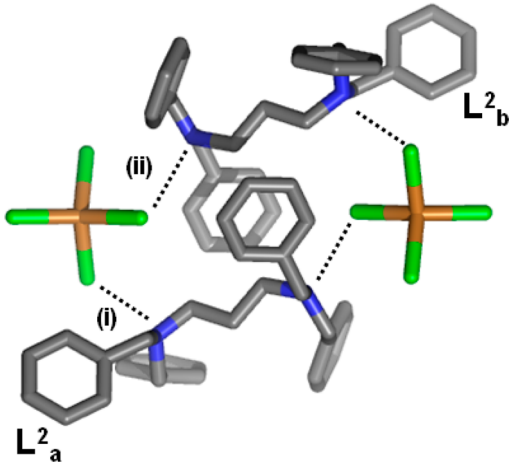

Figure 4. View of the charge-assisted hydrogen bonds (i and ii) between the $[CuCl_4]^{2-}$ dianions and dications in **2**. Clearly, one dication interacts with two different dications (L^2_a and L^2_b). H atoms are omitted for clarity.

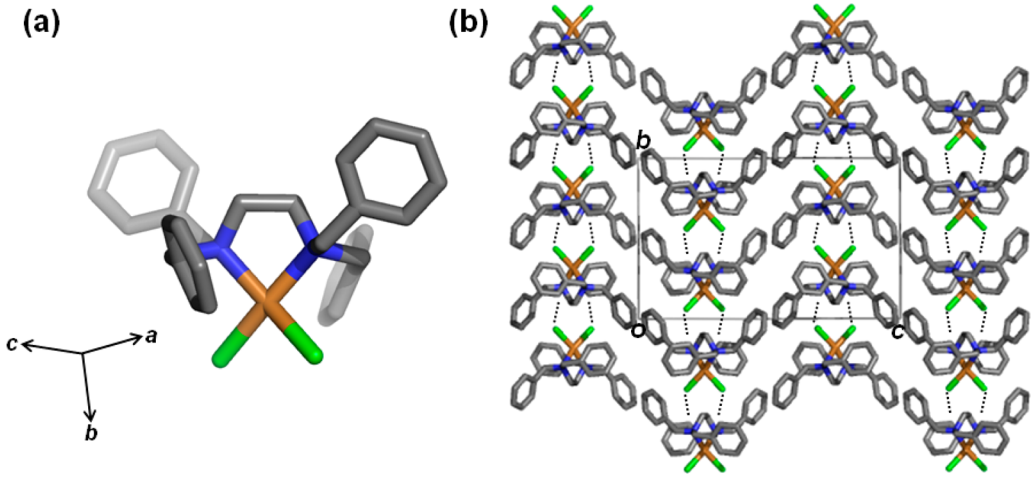

Figure 3. Crystal structure of **1′**. (a) Clamp-shape unit formed upon chelation. (b) Hydrogen-bonded chain along the *b* axis in coordination complex **1′** through C−H···Cl interactions (dashed lines).

dx.doi.org/10.1021/ic5007583 | Inorg. Chem. 2014, 53, 7438−7445

to two different cations (L^2_a and L^2_b) through i and ii charge-assisted N−H···Cl hydrogen bonds. The shortest interaction is i [$d_{N2\cdots Cl4}$ = 3.177(3) Å and angle N2−H102···Cl4 = 167.8(3)°], while ii [$d_{N3\cdots Cl3}$ = 3.207(3) Å and angle N3−H101···Cl3 = 171.3(3)°] is slightly longer. These hydrogen bonds, seemingly divergent, are most likely a result of the longer distance between the N^+ atoms (5.040 Å in salt **2**) in L^2; therefore, the *quasi*-chelating motif is not formed. The other two Cl atoms are involved in weak C−H···Cl interactions with neighboring dications. The disordered nature of the trapped EtOH molecules can be explained by the fact that hydrogen-bonding interactions are not established with either the $[CuCl_4]^{2-}$ dianion or the protonated N atom in the dication.

With this type of anion orientation toward the N atoms in L^2, there is no *quasi*-chelating motif in which one metal center reacts with one dication upon the release of HCl. Indeed, it seems improbable that a chelated ligand such as **1′** could be obtained. To elucidate if the chelated forms, we grinded powders of **2** (31 mg, 0.048 mmol) in the presence of KOH (5.4 mg, 0.096 mmol) for 10 min. Clearly, the diffraction pattern of the product corresponds to a phase that does not match that of salt **2** (Figure 5). The new diffraction pattern is in

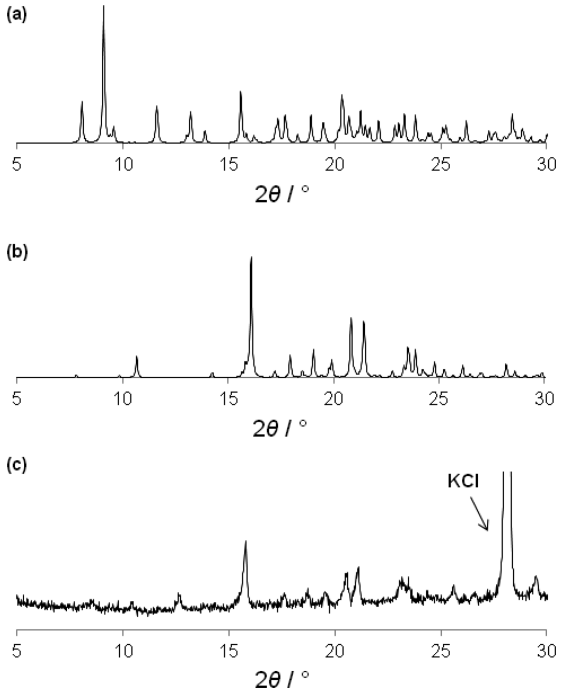

Figure 5. (a) Simulated PXRD pattern of **2** (150 K). (b) Simulated PXRD pattern of ligand L^2 (150 K). (c) PXRD product of **2** grinded in the presence of KOH (298 K). The shift in the diffraction peaks is due to the different temperatures at which the data were recorded.

agreement with that of ligand L^2, confirming that there is no chelated Cu−N bond formation (Figure 5). We also note that there is no color change during grinding, which is expected if chelation occurs. The dehydrochlorination reaction indeed takes place because KCl has been formed (2θ = 28°), after dehydrochlorination between L^2 and KOH.

Then we also investigated the possible mechanochemical reaction by grinding L^2 and $CuCl_2{\cdot}2H_2O$.[17] The PXRD pattern obtained from grinding clearly indicates that the final solid is a mechanical mixture containing L^2 and $CuCl_2{\cdot}2H_2O$, showing that no reaction took place (Figure S5 in the SI). Moreover, recrystallization of the product from EtOH further confirms the presence of L^2.

To ascertain if the longer L^2 ligand chelates upon dehydrochlorination, we set up a crystallization experiment using $HgCl_2$ following the same conditions as those used to crystallize salt **2**. Large colorless single crystals (**3**) crystallizing in the monoclinic $P2_1/c$ space group were obtained.[17] The asymmetric unit consists of one molecule of doubly protonated L^2, one $[HgCl_4]^{2-}$anion, and one molecule of MeOH. In **3**, the two protonated N atoms in L^2 form one charge-assisted hydrogen-bonding interaction (i) [$d_{N1\cdots Cl4}$ = 3.291(6) Å and angle N1−H1···Cl4 = 165.0(4)°] between one protonated N atom of L^2 and $[HgCl_4]^{2-}$ dianions and one N−H···O; [$d_{N2-H2\cdots O1}$ = 2.724(5) Å and angle N2−H2···O1 = 154.7(5)°] interaction (ii) between the other protonated N atom of L^2 and the MeOH molecules (Figure 6a). MeOH acts as a linker

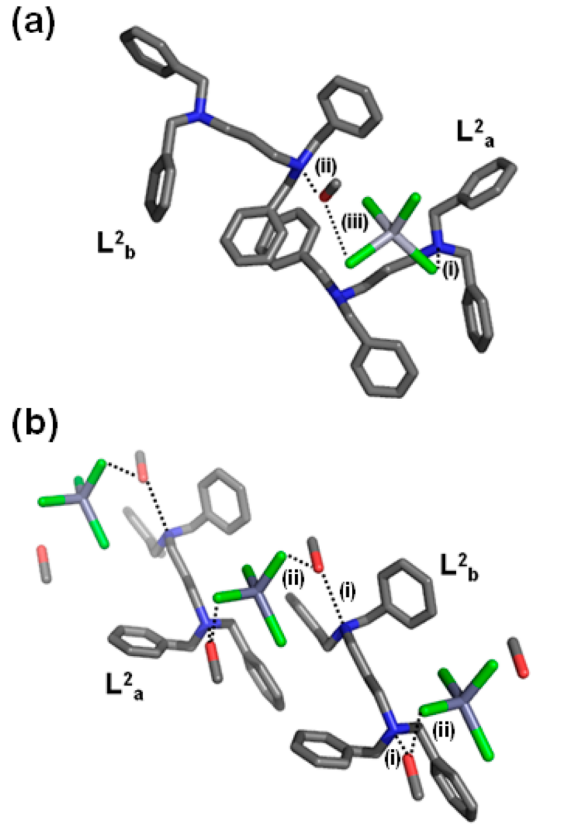

Figure 6. View showing the hydrogen-bonding interactions between the dication and dianion in crystals **3** (a) and **4** (b). H atoms are omitted for clarity.

bridging with another $[HgCl_4]^{2-}$ dianion through a new hydrogen-bonding interaction (iii) [$d_{O1\cdots Cl3}$ = 3.207(5) Å]. Clearly, one dianion interacts with two different dications (L^2_a and L^2_b), being in one case (i.e., ii) mediated through a MeOH molecule (Figure 6a).

The *quasi*-chelating motif observed in **1** is absent in **3** probably because the covalent $N^+{-}N^+$ length (5.015 Å) is longer than the $[HgCl_4]^{2-}$ dianion can accommodate. Therefore, only one Cl of the three in $[HgCl_4]^{2-}$ interacts with the same dication.

To test whether chelation occurs for ligand L^2, we grinded crystals of **3** in the presence of KOH. The PXRD pattern in Figure S7 in the SI shows that salt **3** is maintained after 5 min.

dx.doi.org/10.1021/ic5007583 | Inorg. Chem. 2014, 53, 7438−7445

However, after 10 min, an amorphous phase containing a weak L^2 diffraction is formed. Solution experiments mixing L^2 and $HgCl_2 \cdot H_2O$ did not give a chelating complex.

Replacing Hg^{2+} with Zn^{2+} in the crystallization with L^2 yields a new crystal structure (**4**), showing a different hydrogen-bonding interactions between L^2 and $[ZnCl_4]^{2-}$ anion. One dianion interacts with two different dications (L^2_a and L^2_b) using MeOH as the linking bridge through hydrogen bonds (i) $d_{N1-H1N\cdots O1}$ = 3.068(1) Å and N1−H1N···O1 = 169.8(4)° and (ii) $d_{O1-H10\cdots Cl1}$ = 3.109(1) Å and N1−H1N···O1 = 155.4(7)°. In this case, there is no direct cation−anion interaction. As a result, the *quasi*-chelation motif is not formed (Figure 6b). The new interaction mode is different from that observed in **2** and **3**, which show the structural diversity for this flexible ligand. Mechanochemical grinding of salt **4** with KOH did not form a chelate but L^2 as in the other cases (see Figure S8 in the SI).

Density Functional Theory (DFT) Solid-State QM Calculations. Complementary insights in the field of solid-state reactions can be obtained by theoretical methods, also using QM calculations specific for solid phases. In particular, DFT approaches have been employed herein. The Perdew−Burke−Ernzerhof (PBE)[26] exchange-correlation functions have been used both for gas and solid phases (i.e., under periodical conditions) and, for the sake of consistency, all of the calculations were accomplished by *DMOL*^{3} software.[27]

The combination of a numerical double-ζ quality basis set [including polarization functions on all atoms, i.e., double-ζ numerical with polarization (DNP)] and an effective core potential for the metal atoms was adopted. We assumed experimental X-ray-determined geometries for heavy atoms, while the X−H bond lengths were optimized. A similar computational approach was proven to be adequate in a number of cases such as large supramolecular complexes,[28] systems containing charged particles,[29] and crystalline phases of thiophene-based oligomers and polymers.[30] The effects of intra- and intermolecular interactions have been accounted for by the Grimme scheme with the dispersion DFT (i.e., DFT-D) approach.[31]

In order to assess the reliability of the functional adopted for DFT-D calculations (PBE/DNP plus Grimme contributions), the stabilities of L^1 and L^2 ligands in their crystalline forms have been compared by solid-phase calculations. In accordance with thermal analysis results, the packing of L^1 molecules (mp 98 °C) seemed to be more efficient than that of L^2 molecules (mp 51 °C); i.e., the sublimation energy of the former is higher by ca. 8 kcal mol^{-1}.[32]

DFT-D calculations at the same level involving isolated molecules have been performed to investigate conformational energies and electron distribution of molecules and charged particles possibly involved in the chelating reaction. First of all, it should be underlined once more that in L^1 and L^2 the low-energy structures have a very different N−N distance, evident in both the crystal structures and optimized geometries. In addition, the conformational freedom introduced by an extra methylene group has a strong influence in the cyclic intermediate transition states involved in the chelating reactions.

DFT-D calculations show that the L^1 ligand has a lower proton affinity with respect to that of the L^2 molecule; i.e., the difference in energy between L^1 and protonated L^1 is about 384 kcal mol^{-1}, while this difference increases to 433 kcal mol^{-1} in the case of L^2 (see Tables S1 and S2 in the SI). So, in principle, L^2 can form complexes with metals like the L^1 ligand, which has a lower estimated proton affinity.

However, after deprotonation of the protonated L^1 (that is after removal of $2H^+$ from L^1), the resulting unrelaxed L^1 neutral molecule, which is kept at the geometry of the protonated L^1 but with two H^+ removed, has an energy 35 kcal mol^{-1} higher with respect to the relaxed L^1 neutral molecule. These outcomes can partially justify the ability of L^2 to form a chelate system, lowering its energy.

In addition, the interactions involved in hydrogen-bonded crystals have been analyzed by calculations on small clusters of particles extracted from the X-ray-determined structures. The interaction energy of the dimer representing the *quasi*-chelated motif involving protonated L^1 (see Figure 1a) is ca. 316 kcal mol^{-1}, which is about 158 kcal mol^{-1} for each of the charge-assisted hydrogen bonds. The same calculation has been accomplished to estimate the stability of the two dimers and of the tetramer involving protonated L^2 in Figure 4. The interaction energies are 272 kcal mol^{-1} in the case of a single dimer (involving one hydrogen bond) and 676 kcal mol^{-1} in the case of the tetramer (involving four hydrogen bonds), which is about 169 kcal mol^{-1} for each of the charge-assisted hydrogen bonds. We can easily conclude that protonated L^2 forms (at least locally) stronger hydrogen-bonding interactions than protonated L^1.

Further analysis of DFT outcomes has shown that the more reactive electrons (i.e., electrons in FMOs) in the ligand L^1 with the $-N-CH_2-CH_2-N-$ moiety are essentially localized at the N atoms. As is observed in Figure 7a, the two N lobes in the highest occupied molecular orbitals (HOMOs) are pointing toward the same direction (blue lobes), which we believe is an optimal geometry for establishing the charge-assisted hydrogen bonds with the same $[CuCl_4]^{2-}$ dianion, giving rise to the *quasi*-

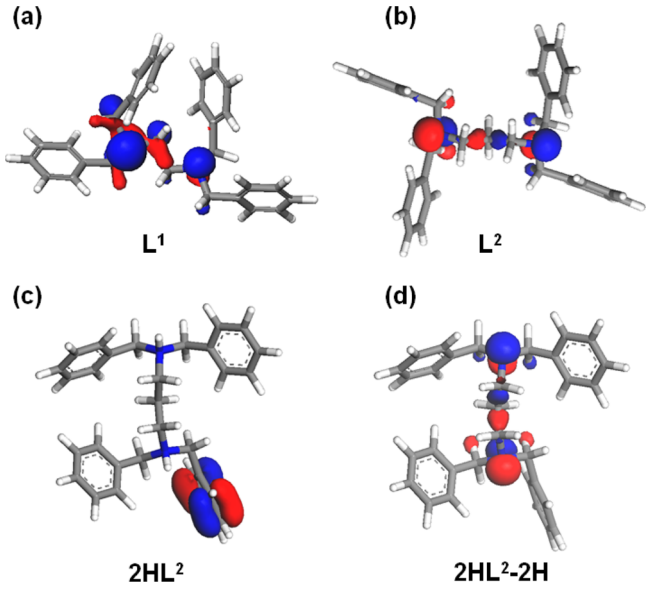

Figure 7. Structures showing the calculated HOMOs in ligand L^2, protonated L^2, and protonated and removed 2H. For ligand L^1, the case of protonated and removed 2H is presented part a. Clearly, in L^1, the orientation of the HOMOs is in the same direction, while in L^2, the orientation of the lobes is in such a way that rotation of one N group is necessary if a coordination reaction takes place (i.e., opposite direction). In $2HL^2$, clearly the HOMOs are displaced to the pendant phenyl rings.

dx.doi.org/10.1021/ic5007583 | Inorg. Chem. 2014, 53, 7438−7445

chelated motif in complex **1**. Upon grinding of **1** in the presence of KOH, this optimal orientation facilitates the formation of a chelated complex via a dehydrochlorination reaction.

Gas-phase DFT calculations also show that the FMO distribution is localized around the $-N-CH_2-CH_2-CH_2-N-$ group in crystals **2**–**4**. The conformations of ligand $\mathbf{L}^2$ in the crystal of pure $\mathbf{L}^2$ and of $\mathbf{L}^2$ (**2**) nonchelating are quite different. Obviously, the nonchelating structure contains the $\mathbf{L}^2$ molecules with protonated N atoms. As shown in Figure S9 in the SI, the different dihedral angles of the pendant phenyl groups in pure $\mathbf{L}^2$ compared to the nonchelating without the two N protons in ligand $\mathbf{L}^2$ is quite considerable. However, both structures have a N–N distance too large to be coordinated to form a chelated complex [d_{N-N} = 5.113 (5.040) vs 3.766 (3.683) Å of the $-N-CH_2-CH_2-N-$ backbone]. Moreover, the N lone pairs are directed away with respect to a hypothetical complexing metal approaching the system.

In $\mathbf{L}^2$, the HOMO is localized essentially at the N atoms (Figure 7b), while after N protonation (Figure 7c), the HOMO is displaced by the phenyl moieties. It should be emphasized that, even if the HOMOs of $\mathbf{L}^2$ (Figure 7b) and $\mathbf{L}^2$ nonchelating without H^+ (Figure 7d) reside on the N atoms, the distribution does not allow the formation of a chelate without a relative rotation of the N groups to orient the HOMO lobes properly.[33] In fact, for symmetry reasons (the HOMOs have π symmetry), the lobes of the terminal N atoms have opposite signs, at variance with the case of $\mathbf{L}^1$ (Figure 7a). In conclusion, the number of CH_2 groups between N atoms in stable conformations of $\mathbf{L}^1$ and $\mathbf{L}^2$ not only influences the distance between the N atoms but also plays a role in the symmetry of the corresponding HOMOs. Both of these effects seem to support the experimental outcomes relating to the reticent tendency of $\mathbf{L}^2$ to chelate upon dehydrochlorination.

CONCLUSIONS

In summary, we have monitored the solid-state dehydrochlorination reaction using bidentate large flexible ligands with different backbone chain lengths (i.e., two and three $-CH_2-$ units). In the solid state, when the backbone length is ca. 3.8 Å (ethylenic backbone), a *quasi*-chelating motif involving two Cu–Cl···H–N interactions from one $[CuCl_4]^{2-}$ dianion and the two protonated N atoms of one dication is observed. This allows dehydrochlorination reaction upon grinding in the presence of KOH to give a neutral coordination complex. However, for the ligand with longer backbone chains length (propylenic) of ca. 5 Å, the *quasi*-chelating motif was not formed. In such cases, one M–Cl (where M = Cu, Hg, and Zn) interacts with one protonated N atom of the dication, forcing the anion to split the second M–Cl···H–N interactions to another dication. In those cases, the chelating reaction upon grinding with KOH does not occur, as shown by PXRD. The experimental results have been further corroborated and explained by DFT calculations both in the solid state and in the gas phase, demonstrating that the effect of conformational energies, intermolecular interactions, and electron distribution in the FMOs and their symmetry also can play an important role in the reactivity of $\mathbf{L}^1$ and $\mathbf{L}^2$. We believe that the combination of X-ray crystallography and DFT calculations in the solid state has a great potential to study and probably predict reactions of the type described here.

Currently, we are actively working on the design and synthesis of functional porous hybrid metal organic salts by combining second-sphere coordination and mechanochemical dehydrochlorination reactions by means of crystal engineering.

ASSOCIATED CONTENT

Supporting Information

Further details on the synthesis and crystallographic information. This material is available free of charge via the Internet at http://pubs.acs.org.

AUTHOR INFORMATION

Corresponding Authors

*E-mail: fguo@lnu.edu.cn.

*E-mail: javier.rujas@iit.it.

Author Contributions

The manuscript was written through contributions of all authors. All authors have given approval to the final version of the manuscript.

Notes

The authors declare no competing financial interest.

ACKNOWLEDGMENTS

This research was supported by the NSFC (Grants 20903052 and 20772054), the program for Liaoning excellent talents in University (Grant LJQ 2011003), the innovative team project of education department of Liaoning Province (Grant LT2011001), and Liaoning University (Grant 2012LDGY06). A.F. acknowledges CINECA for computational resources through a Laboratory for Interdisciplinary Advanced Simulation Initiative 2013 grant (Projects SIMFO and QMC_opt) and CARIPLO for financial support (Project PLENOS). J.M.-R. thanks the Italian Institute of Technology for financial support.

REFERENCES

(1) (a) Desiraju, G. R.; Vittal, J. J.; Ramanan, A. *Crystal Engineering: A Textbook*; World Scientific: Singapore, 2011. (b) Desiraju, G. R. *J. Am. Chem. Soc.* **2013**, *135*, 9952–9967.

(2) Vishweshwar, P.; McMahon, J. A.; Peterson, M. L.; Hickey, M. B.; Shattock, T. R.; Zaworotko, M. J. *Chem. Commun.* **2005**, 4601–4603.

(3) (a) Reddy, D. S.; Duncan, S.; Shimizu, G. K. H. *Angew. Chem., Int. Ed.* **2003**, *42*, 1360–1364. (b) Dalrymple, S. A.; Shimizu, G. K. H. *J. Am. Chem. Soc.* **2007**, *129*, 12114–12116. (c) Noro, S.-i.; Fukuhara, K.; Sugimoto, K.; Hijikata, Y.; Kubo, K.; Nakamura, T. *Dalton Trans.* **2013**, *42*, 11100–11110.

(4) Sokolov, A. N.; Friščić, T.; MacGillivray, L. R. *J. Am. Chem. Soc.* **2006**, *128*, 2806–2807.

(5) (a) Martí-Rujas, J.; Desmedt, A.; Harris, K. D. M.; Guillaume, F. *J. Phys. Chem. B* **2006**, *110*, 10708–10713. (b) Martí-Rujas, J.; Desmedt, A.; Harris, K. D. M.; Guillaume, F. *J. Phys. Chem. B* **2007**, *111*, 12339–12344. (c) Martí-Rujas, J.; Desmedt, A.; Harris, K. D. M.; Guillaume, F. *J. Phys. Chem. C* **2009**, *113*, 736–743.

(6) (a) Coulquhoun, H. M.; Lewis, D. F.; Stoddart, J. F.; Williams, D. J. *Dalton Trans.* **1983**, *4*, 607–613. (b) Colquhoun, H. M.; Doughty, S. M.; Stoddart, J. F.; Williams, D. J. *Angew. Chem., Int. Ed. Engl.* **1984**, *23*, 235–236. (c) Alston, D. R.; Slawin, A. M. Z.; Stoddart, J. F.; Williams, D. J. *Angew. Chem., Int. Ed. Engl.* **1985**, *24*, 786–787. (d) Colquhoun, H. M.; Stoddart, J. F.; Williams, D. J. *Angew. Chem., Int. Ed. Engl.* **1986**, *25*, 487–507.

(7) (a) Loeb, S. J. In *Comprehensive Supramolecular Chemistry*; Atwood, J. L., Davies, J. E. D., MacNicol, D. D., Vögtle, F., Eds.; Elsevier Science: New York, 1996; Vol. *1*, p 733. (b) Beauchamp, D. A. S.; Loeb, J. *Chem.—Eur. J.* **2002**, *8*, 5084–5088. (c) Mercer, D. J.; Loeb, S. J. *Chem. Soc. Rev.* **2010**, *39*, 3612–3620.

(8) (a) Warr, R. J.; Westra, A. N.; Bell, K. J.; Chartres, J.; Ellis, R.; Tong, C.; Simmance, T. G.; Gadzhieva, A.; Blake, A. J.; Tasker, P. A.; Schröder, M. *Chem.—Eur. J.* **2009**, *15*, 4836−4850. (b) Turkington, J. R.; Cocalia, V.; Kendall, K.; Morrison, C. A.; Richardson, P.; Sassi, T.; Tasker, P. A.; Bailey, P. J.; Sole, K. C. *Inorg. Chem.* **2012**, *51*, 12805−12819. (c) Ellis, R. J.; Chartres, J.; Sole, K. C.; Simmance, T. G.; Tong, C. C.; White, F. J.; Schröder, M.; Tasker, P. A. *Chem. Commun.* **2009**, *5*, 583−585.

(9) Liu, Z.; Frasconi, M.; Lei, J.; Brown, Z. J.; Zhu, Z.; Cao, D.; Iehl, J.; Liu, G.; Fahrenbach, A. C.; Farha, O. K.; Hupp, J. T.; Mirkin, C. A.; Botros, Y. Y.; Stoddart, J. F. *Nat. Commun.* **2013**, *4*, 1855−1864.

(10) (a) Metrangolo, P.; Neurkich, H.; Pilati, T.; Resnati, G. *Acc. Chem. Res.* **2005**, *38*, 386−395. (b) Rissanen, K. *CrystEngComm* **2008**, *10*, 1107−1113.

(11) Abate, A.; Martí-Rujas, J.; Metrangolo, P.; Pilati, T.; Resnati, G.; Terraneo, G. *Cryst. Growth Des.* **2011**, *11*, 4220−4226.

(12) Guo, F.; Shao, H. D.; Yang, Q.; Famulari, A.; Martí-Rujas, J. *CrystEngComm* **2014**, *16*, 969−973.

(13) (a) MacGillivray, L. R. *Metal Organic Frameworks: Design and Applications*; Wiley: New York, 2010. (b) Eddaoudi, M.; Moler, D. B.; Li, H.; Chen, B.; Reineke, T. M.; O'Keeffe, M.; Yaghi, O. M. *Acc. Chem. Res.* **2001**, *34*, 319−330. (c) Kitagawa, S.; Kitaura, R.; Noro, S.-i. *Angew. Chem., Int. Ed.* **2004**, *43*, 2334−2375. (d) Ferey, G. *Chem. Soc. Rev.* **2008**, *37*, 191−214. (e) Inokuma, Y.; Kawano, M.; Fujita, M. *Nat. Chem.* **2010**, *3*, 349−358. (f) Martí-Rujas, J.; Kawano, M. *Acc. Chem. Res.* **2013**, *46*, 493−505.

(14) (a) Hosseini, M. W. *Acc. Chem. Res.* **2005**, *38*, 313−323. (b) Dechambenoit, P.; Ferlay, S.; Kyritsakas, N.; Hosseini, M. W. *J. Am. Chem. Soc.* **2008**, *130*, 17106−17113. (c) Coronado, E.; Giménez-Marqués, M.; Espallargas, G. M.; Brammer, L. *Nat. Commun.* **2012**, *3*, 828−836. (d) Ferlay, S.; Dechambenoit, P.; Kyritsakas, N.; Hosseini, W. K. *Dalton Trans.* **2014**, *43*, 158−165.

(15) (a) James, S. L.; Adams, C. J.; Bolm, C.; Braga, D.; Collier, P.; Friščić, T.; Grepioni, F.; Harris, K. D. M.; Hyett, G.; Jones, W.; Krebs, A.; Mack, J.; Maini, L.; Orpen, A. G.; Parkin, I. P.; Shearouse, W. C.; Steed, J. W.; Waddell, D. C. *Chem. Soc. Rev.* **2012**, *41*, 413−447. (b) Friščić, T. *Chem. Soc. Rev.* **2012**, *41*, 3493−3510.

(16) (a) Sheldrick, G. M. *SHELXTL Reference Manual*; Siemens Analytical X-ray Systems, Inc.: Madison, WI, 1996. (b) Sheldrick, G. M. *Acta Crystallogr.* **2008**, *A64*, 112−122.

(17) See the SI for further information.

(18) Pan, Z.; Zhang, M.; Yuan, D.; Ma, P. *Acta Crystallogr., Sect. E* **2005**, *E61*, o185−o186.

(19) We have observed that, if the single-crystal X-ray data collection of **1** is recorded at 175 K, a monoclinic unit cell is obtained. The new phase shows a stoichiometric ratio of 1:1:2 (cation/anion/EtOH), while the charge-assisted hydrogen bonds are practically the same.

(20) We define a *quasi*-chelating building block when a $[CuCl_4]^{2-}$ is hydrogen-bonded to the same cation through two N−H···Cl hydrogen bonds, which upon dehydrochlorination reaction can yield a coordination complex.

(21) We note that, in the bidentate ligand with *p*-methoxy groups in the phenyl rings, the *quasi*-chelated unit adopts a clamp-shaped conformation, which is quite different from that observed in **1**. See ref 12.

(22) (a) Espallargas, G. M.; Brammer, L.; Van de Streek, J.; Shankland, K.; Florence, A. J.; Adams, H. *J. Am. Chem. Soc.* **2006**, *128*, 9584−9585. (b) Adams, C. J.; Colquhoun, H. M.; Crawford, P. C.; Lusi, M.; Orpen, A. G. *Angew. Chem., Int. Ed.* **2007**, *46*, 1124−1128.

(23) (a) Adams, C. J.; Kurawa, M. A.; Lusi, M.; Orpen, A. G. *CrystEngComm* **2008**, *10*, 1790−1795. (b) Adams, C. J.; Gillon, A. L.; Lusi, M.; Orpen, A. G. *CrystEngComm* **2010**, *12*, 4403−4409. (c) Adams, C. J.; Haddow, M. F.; Lusi, M.; Orpen, A. G. *CrystEngComm* **2011**, *13*, 4324−4331.

(24) LAG refers to the mechanical reaction aided by the addition of stoichiometric amounts of solvent.

(25) Single-crystal XRD reveals that $\mathbf{L}^2$ crystallizes in the $P2_1/c$ space group, and the main interactions stabilizing the molecules in the unit cell are mainly weak C−H···π contacts, which explains why $\mathbf{L}^2$ melts at ca. 50 °C (see Figure S4 in the SI).

(26) (a) Perdew, J. P.; Burke, K.; Ernzerhof, M. *Phys. Rev. Lett.* **1996**, *77*, 3865−3868. (b) Perdew, J. P.; Burke, K.; Ernzerhof, M. E. *Phys. Rev. Lett.* **1997**, *78*, 1396−1396.

(27) Delley, B. *J. Chem. Phys.* **2000**, *113*, 7756−7764 . *Materials Studio* and *DMOL*^{3} are Accelerys Inc. products (see www.accelrys.com)..

(28) (a) Kolokoltsev, Y.; Amelines-Sarria, O.; Gromovoy, T. Y.; Basiuk, V. A. *J. Comput. Theor. Nanosci.* **2010**, *7*, 1095−1103. (b) Amelines-Sarria, O.; Kolokoltsev, Y.; Basiuk, V. A. *J. Comput. Theor. Nanosci.* **2010**, *7*, 1996−2003. (c) Basiuk, V. A.; Amelines-Sarria, O.; Kolokoltsev, Y. *J. Comput. Theor. Nanosci.* **2010**, *7*, 2322−2330. (d) Basiuk, V. A. *Int. J. Quantum Chem.* **2011**, *15*, 4197−4205.

(29) (a) Yu, G.; Yin, S.; Liu, Y.; Shuai, Z.; Zhu, D. *J. Am. Chem. Soc.* **2003**, *125*, 14816. (b) Guo, F.; Zhang, M.-Q.; Famulari, A.; Martí-Rujas, J. *CrystEngComm* **2013**, *15*, 6237−6243. (c) Maccaroni, E.; Malpezzi, L.; Famulari, A.; Masciocchi, N. *J. Pharmaceut. Biomed. Anal.* **2012**, *60*, 65−70.

(30) (a) Famulari, A.; Raos, G.; Baggioli, A.; Casalegno, M.; Po, R.; Meille, S. V. *J. Phys. Chem. B* **2012**, *116*, 14504−14509. (b) Casalegno, M.; Baggioli, A.; Famulari, A.; Meille, S. V.; Nicolini, T.; Po, R.; Raos, G. *EPJ Web Conf.* **2012**, 02002-1−02002-8, DOI: 10.1051/epjconf/20123302002. (c) Nicolini, T.; Famulari, A.; Gatti, T.; Martí-Rujas, J.; Villafiorita Monteleone, F.; Canesi, E. V.; Meinardi, F.; Botta, C.; Parisini, E.; Meille, S. V.; Bertarelli, C. *J. Phys. Chem. Lett.* **2014**, *5*, 2171−2176.

(31) (a) Grimme, S. *J. Chem. Phys.* **2006**, *124*, 34108−34134. (b) Baggioli, A.; Meille, S. V.; Raos, G.; Po, R.; Brinkmann, M.; Famulari, A. *Int. J. Quantum Chem.* **2013**, *113*, 2154−2162. (c) Baggioli, A.; Famulari, A. *Phys. Chem. Chem. Phys.* **2014**, *16*, 3983−3994.

(32) From the X-ray structures, it is possible to observe that $\mathbf{L}^1$ and $\mathbf{L}^2$ show structural diversity because the crystal packing is the same in both structures, with the only difference being the weak C−H···C interactions in $\mathbf{L}^2$ [$d_{H4\cdots C7A^*}$ = 2.880(3) Å and angle C2−H4···C7A* = 139.0(2)°]. In $\mathbf{L}^1$, such interactions [$d_{H6\cdots C14}$ = 2.871(2) Å and angle C21−H6···C14 = 142.9(1)°] are stronger than those in $\mathbf{L}^2$. Variation in the stability is caused by the addition of one CH_2 group in the ethylenic backbone, which results in distortion of the C−H···C interactions between adjacent ligands. For structural diversity, see: Martí-Rujas, J.; Kariuki, B. M.; Hughes, C. E.; Morte-Ródenas, A.; Guo, F.; Glavcheva-Laleva, Z.; Tatsemur, K.; Ooi, L.; Yeo, L.; Harris, K. D. M. *New J. Chem.* **2011**, *35*, 1515−1521.

(33) We computed the HOMOs for the diprotonated $\mathbf{L}^2$ but after removal of the two H atoms at the N atoms because this could be seen as a potential contributor to the transition state during an eventual dehydrochlorination reaction. The absence of chelation can be explained as due to inappropriately oriented HOMOs.